Applied Thermal Engineering 146 (2019) 243–251

Contents lists available at ScienceDirect

Applied Thermal Engineering

journal homepage: www.elsevier.com/locate/apthermeng

Research Paper

Thermo-mechanical behavior of energy diaphragm wall: Physical and numerical modelling

Shengshi Dong[a], Xiaozhao Li[a,*], Anh Minh Tang[b], Jean Michel Pereira[b], Van Tri Nguyen[b], Ping Che[c], Zhiyong Xiong[a]

[a] School of Earth Sciences and Engineering, Nanjing University, Zhugongshan Building, Xianlin Avenue, Nanjing, Jiangsu Province 210023, PR China
[b] Laboratoire Navier, UMR 8205, École des Ponts ParisTech, IFSTTAR, CNRS, UPE, France
[c] East China Mineral Exploration and Development Bureau, Nanjing, Jiangsu Province 210007, PR China

HIGHLIGHTS

- The mechanism of thermo-mechanical behavior of energy diaphragm wall is interpreted.
- Thermal dilation bends the wall causing different mechanical responses on both sides.
- A 2D model is proposed to predict the thermo-mechanical behavior of energy wall.

ARTICLE INFO

Keywords:
Thermo-mechanical behavior
Energy diaphragm wall
Physical model
Numerical simulation

ABSTRACT

The paper presents a study of the thermo-mechanical behavior of energy diaphragm wall. A physical model, which consists of a small-scale concrete diaphragm wall equipped with a heating exchange pipe, was used. A heating test was performed where hot water (at 50 °C) was circulated through a heat exchange pipe for 75 h. The results show that the temperatures in the wall and in the soil increased quickly during the first 20 h and reached stabilization at the end of the experiment. The temperature increase induced increase of axial strain in the wall and earth pressure at the soil/wall interface. In addition to the experiment, a numerical model, using finite element analysis, was used to predict the behavior of the wall during this experiment. The good agreement between the numerical and the experimental results allows the main phenomena that took place to be explained; heating induces thermal expansion of the wall that results in the modification in stress in the wall and at the soil/wall interface. In addition, since the pipe was located closer to one side of the wall, the thermal expansion of the wall was not homogenous, and the wall bent during heating.

1. Introduction

A thermo-active (or energy) geostructure is a new-style Ground Source Heat Pump (GHSP) system that includes conventional geostructures (*e.g.* pile foundation, tunnel lining, diaphragm wall) with individual or several pipe circuits (high-density polyethylene pipes, HDPE) embedded within as primary circuit to enable heat exchange with the surrounding ground [1]. In winter, heat is extracted from the ground for the purpose of heating and in summer, heat is injected into the ground to provide cooling. Energy geostructures are considered an interesting and promising technology to tackle the increasing energy demands for heating and cooling of buildings and other infrastructures, by making use of it as a local and sustainable source. However, there are still concerns about the thermal exchange, between the structure and the ground, which may induce variation in the stress/strain behavior of the geostructure and, as a consequence, be a threat to its safety and performance. Thus, several research works have been focused on the thermo-mechanical behavior of energy geostructures in order to better understand its stress/strain behavior under combined thermal and mechanical loading [2–8].

However, most of the existing studies are related to the thermo-mechanical behavior of energy piles. The methods used include in situ experiments [9–12], laboratory tests [13–23] and numerical simulations [24–29]. It has been reported that there are significant changes in stress distribution and shaft resistance due to constraints on the thermal expansion/contraction [30]. Although these phenomena are not expected to lead to detrimental consequences, they should be taken into consideration at the design stage.

* Corresponding author at: Nanjing University, No. 163 Xianlin Avenue, Nanjing, 210023 Jiangsu Province, PR China.
E-mail address: lixz@nju.edu.cn (X. Li).

https://doi.org/10.1016/j.applthermaleng.2018.09.054
Received 17 September 2017; Received in revised form 14 August 2018; Accepted 10 September 2018
Available online 11 September 2018
1359-4311/

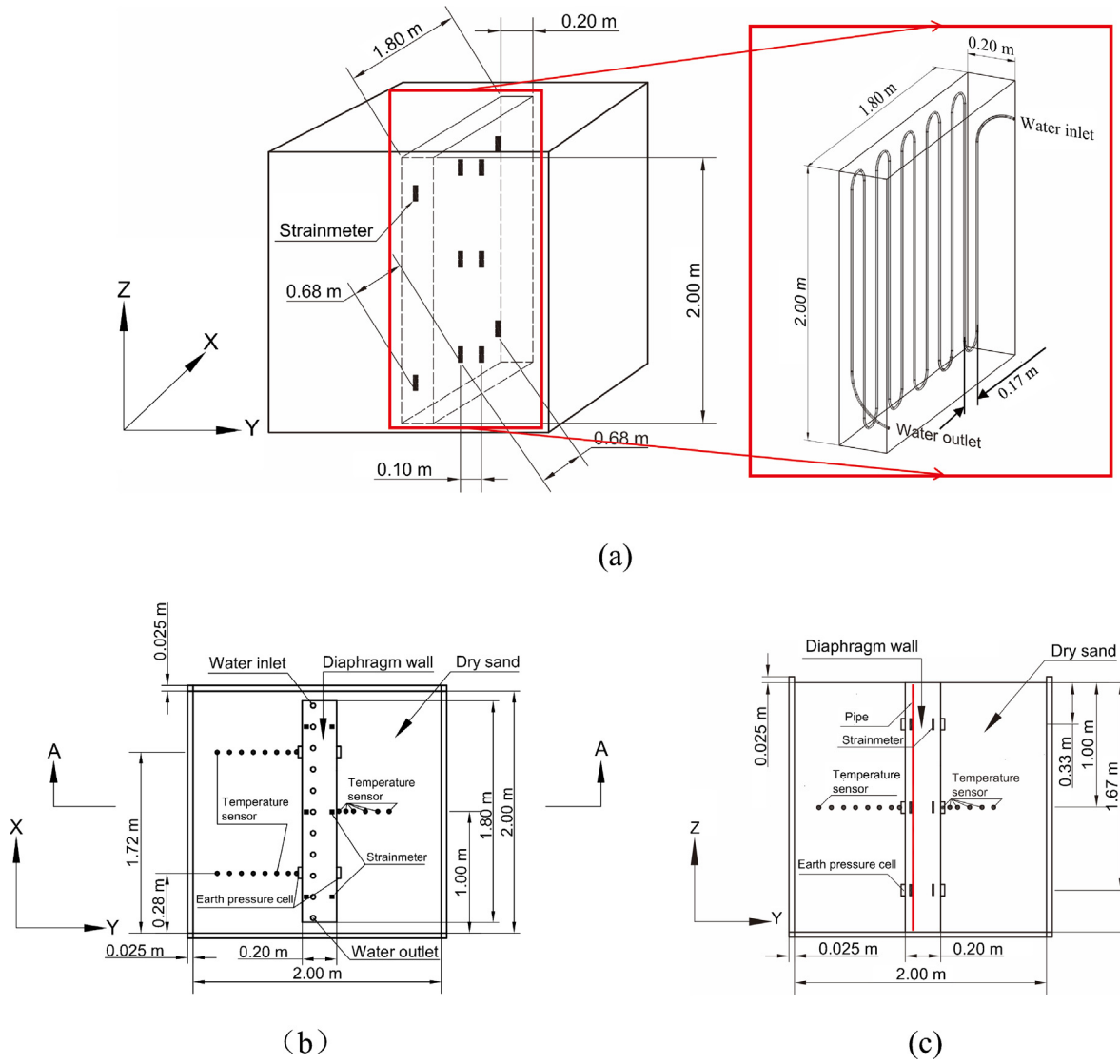

Fig. 1. Schematic view of the experimental setup; (a) 3D view of the physical model with the details of the pipe and strainmeters; (b) Horizontal section at Z = 1.00 m; (c) Section A-A, Vertical section at X = 1.00 m.

Table 1
Detailed information of sensors.

Sensor	Market model No.	Specification	Capacity	Sensibility	Error
Earth pressure cell	JTM-V2000	Vibrating wire	300 kPa	≤0.24 kPa	≤1 kPa
Strainmeter (embedment)	BGK-4200	Vibrating wire	3000 με	1 με	≤3 με
Temperature sensor	Pt100	Thermal resistance	0–300 °C	≤0.04%	0.3 °C

Few studies of the thermo-mechanical performance of energy diaphragm walls have been published however [31,32]. It has been suggested that thermally-induced strains and stresses also develop in energy walls [32]. However, their effects are less predictable than in energy piles because of their greater complexity in terms of geometry. Sterpi et al. [32] performed 3D thermo-mechanical Finite Element Analyses (FEA) and concluded that the thermally induced effects on the structure were not negligible and could be observed partly as additional displacements, partly as variations of the internal actions. Bourne-Webb et al. [31] also performed numerical simulations and found that changes to the wall mechanical response were dominated by seasonal temperature changes.

The most important function of the diaphragm wall is for ground support and seepage control. If there is crack in the wall, the deformation caused by thermal expansion/contraction and lateral soil pressure may aggravate the damage. Some diaphragm walls are also applied for bearing purpose, as a result, the thermally-induced strains and stresses are thus important to be investigated. Numerical analysis have demonstrated an increase of radial contact pressures on the soil-pile interface due to temperature-induced expansion of the pile [33,34]. For energy pile, this increase of radial contact pressures could only increase the soil-pile frictional resistance. But for diaphragm wall, due to the existence of excavation at one side of the wall, the pressure change may cause additional deformation after Sterpi et al. [32]. However, the bending moment caused by heating was small and overwhelmed by the effect of environmental thermal boundary conditions through numerical analysis by Bourne-Webb et al. [31].

This paper presents a study to evaluate the thermo-mechanical response of an energy diaphragm wall by using physical and numerical modeling. A small-scale energy diaphragm wall was installed in dry sand. Its behavior under thermal loading was monitored using strain, stress and temperature sensors embedded inside/on the wall and also in

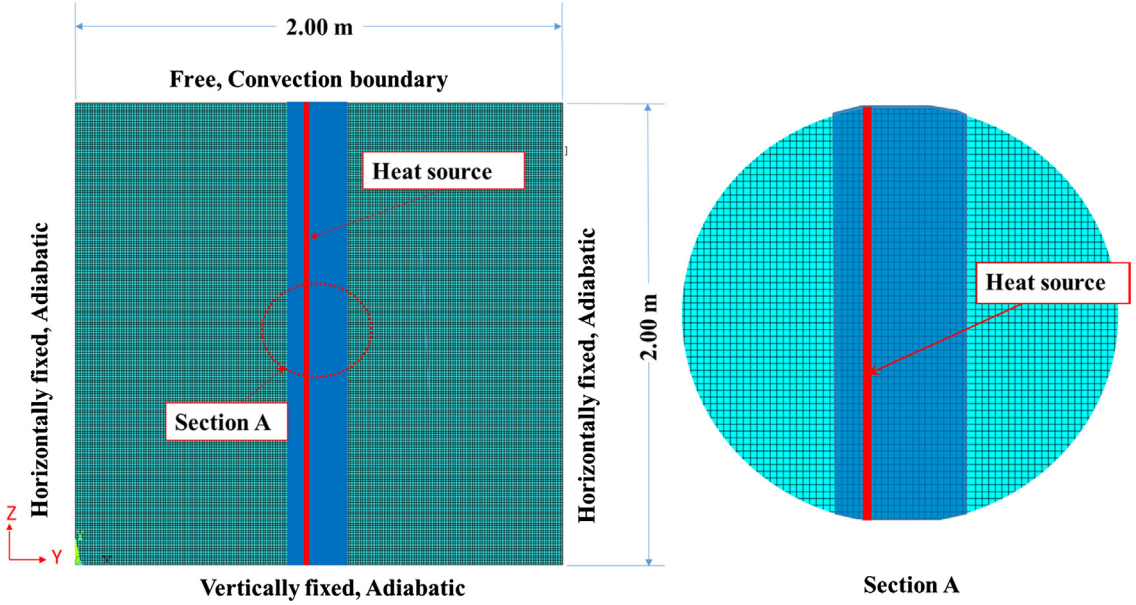

Fig. 2. Finite element mesh and boundaries conditions used for the numerical simulations.

Table 2
Materials parameters used for simulation.

Parameter	Cement mortar	Dry sand
Thermal conductivity (W/(m K))	1.20	0.32
Density (Mg/m^3)	1.55	1.62
Specific heat (J/(kg K))	736	700
Young's modulus (MPa)	12,000	50
Poisson's ratio (–)	0.20	0.26
Coefficient of linear expansion (με/°C)	10	6
Cohesion (kPa)	–	0.1
Friction angle (°)	–	30
Dilation angle (°)	–	4

the surrounding soil. At the same time, its behavior was predicted by using Finite Element Analyses (FEA). The combination of the two methods allows better understanding the thermo-mechanical behavior of an energy diaphragm wall when its temperature is varied.

2. Physical model

The schematic view of the physical model is shown in Fig. 1. A small-scale concrete diaphragm wall (2.00 m high, 1.80 m wide, and 0.20 m thick) was installed inside a steel box and the bottom of the wall was in contact with the bottom of the box. The internal height and width of the box are similar to those of the wall. The thickness of the box walls and floor is 25 mm with other 30 mm grillage structure outside, which is large enough to consider that the box is rigid. The box was exposed to the indoor air with a controlled temperature of 10 ± 2 °C and the heat convection between the surfaces and air is natural convection. Prior to the experiment, the box was filled with dry sand in layers of 0.2-m thickness which were compacted to a density of about 1.62 Mg/m^3 (corresponding to a relative density of 80% and void ratio of 0.63). The control of density by layer ensures its uniformity throughout the test specimen. This physical model can be considered representative of the wall below the internal excavation level. As a result, the effect of the thermal boundary conditions on the thermo-mechanical behavior, identified in other studies [30,31], will not be captured.

The soil temperature was measured at various locations located on a plane at 1-m depth (see Fig. 1c). At this depth, the temperature sensors were distributed in three lines, two on the left-hand side and one on the right-hand side (see Fig. 1b). This allows the soil temperature to be measured at different distances from the diaphragm wall surfaces at the same depth. The diaphragm wall was equipped with high-density polyethylene pipes (10 mm in external diameter and 8 mm in internal diameter) to distribute the heating fluid, and various sensors to measure earth pressure, temperature and strain. The details are shown in Fig. 1. The pipes were distributed on a plan located at 0.05 m from the left-hand side surface of the wall and the distance between the pipes was 0.17 m (see Fig. 1b, c). The details of the pipe arrangement are shown in Fig. 1a. To measure the earth pressure at the soil/wall interface, 12 sensors were used. These sensors were distributed at three depths (0.33 m, 1.00 m, and 1.67 m) (see Fig. 1c). At each depth, two sensors were located on each side of the wall (see Fig. 1b). Several strainmeters were tied to the rebars, as shown in Fig. 1a, to measure the strain at various locations inside the wall. Note that the strainmeters and the earth pressure transducers have integrated with thermistors to measure the temperature. The characteristics of the sensors used are shown in Table 1 and the calibrations and corrections for the temperature were done by the producers and considered in the data processing. The wall was fabricated outside of the box. After 30 days of curing, it was then installed inside the box and the earth pressure and soil temperature sensors were installed during the compaction of dry sand to fill the box.

After the installation of the experiment, heating was applied to the wall by circulating water through the pipes at a temperature of 50 °C and with a flow rate of 0.03 m^3/h, for a period of 75 h. Beside the temperature evolution which was measured at various locations inside the wall and in the soil, earth pressures at the soil/wall interface and strains inside the wall were also recorded.

3. Numerical model

In order to predict the mechanical behavior of the wall during this experiment, Finite Element Analysis (FEA) (using ANSYS) was under taken. The 2D mesh, plotted in Fig. 2, represents the section shown in Fig. 1c. Plane strain conditions were applied corresponding to the boundary conditions of the experiment. The horizontal displacements at the left-hand side and the right-hand side were restrained. The vertical displacement at the bottom of the mesh was also restrained while the stress applied to the top of the mesh was null. The downward vertical displacement at the base of the wall was restrained but the horizontal displacement was not. According to the experimental results,

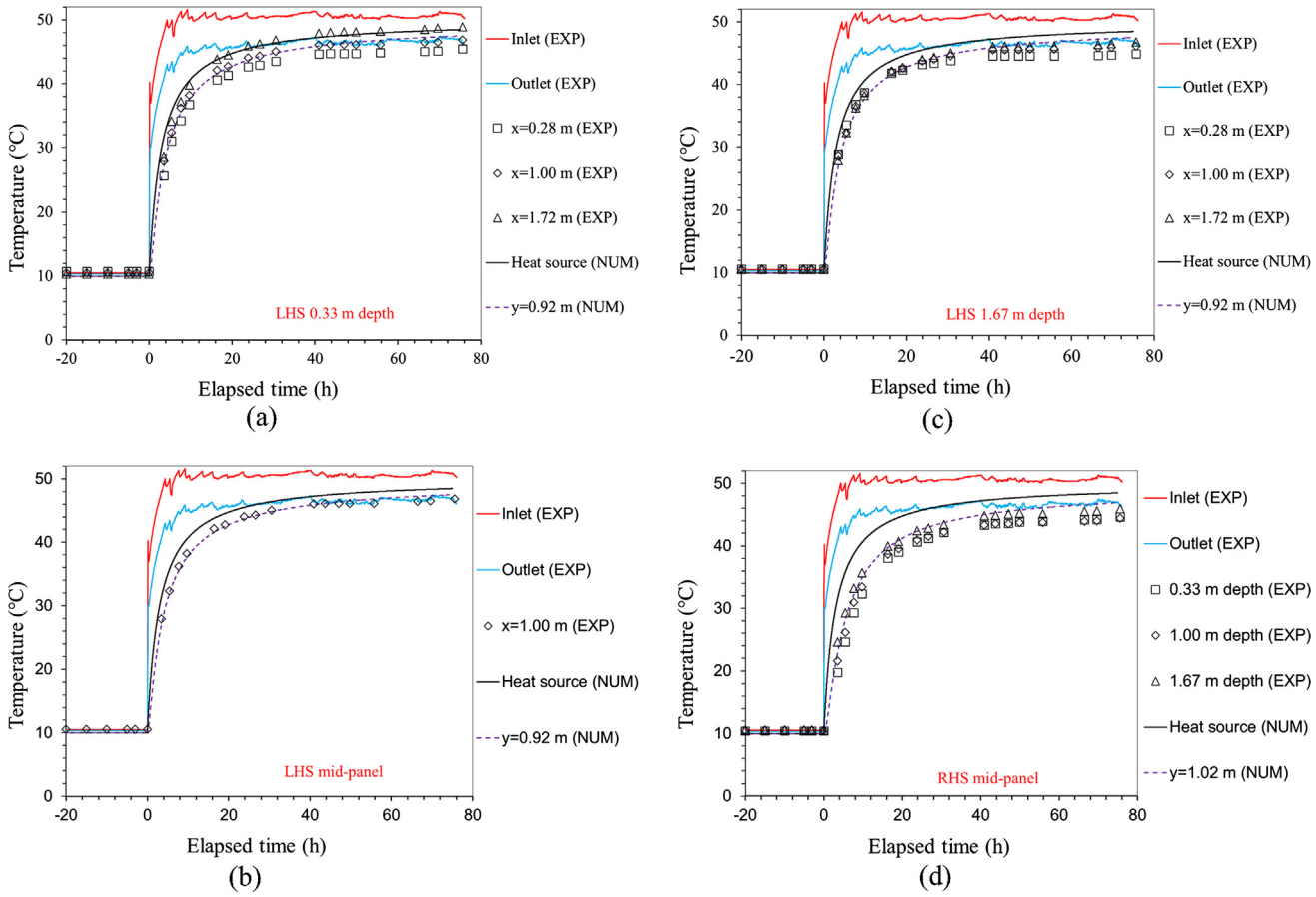

Fig. 3. Temperature versus elapsed time within the wall on the left-hand side along the x coordinate at depth of (a) 0.33 m and (b) 1.00 m and (c) 1.67 m and (d) on the right-hand side at x = 1.00 m for various depths.

the thermal boundary conditions on the left-hand side and right-hand side have only small influence on the temperature distribution. For this reason, the thermal boundary conditions on these two sides were supposed to be adiabatic. Heat flux was equally supposed to be negligible at the bottom boundary. On the top of the model, thermal convection boundary was set with an air temperature of 10 °C and a convective heat transfer coefficient of 2.5 W/(m^2 K) ([31]), as it was open to the air.

The governing laws used in this study are summarized as follows: (*i*) only conduction was considered for heat transfer; (*ii*) the mechanical behavior of the wall was linear elastic while that of the soil was elasto-plastic with the Drucker-Prager yield criterion; (*iii*) the thermo-mechanical behavior of the wall and soil was linear elastic. The material parameters used for the simulation are shown in the Table 2. Among the parameters, the density, thermal conductivity and specific heat of cement mortar and sand used in the FEA were measured by specialized equipment and also calibrated by one dimensional finite difference method with MATLAB. The Young's modulus and Poisson's ratio of cement mortar were measured by elastic modulus test machine. Other parameters of cement mortar and sand were taken from the literatures ([35–37]). It should be stated that the coefficient of linear expansion was chosen at $0.6 \times 10^{-5}\,°C^{-1}$ from literature [35], which gives a typical linear thermal expansion coefficient for dense quartzose sands from $0.6 \times 10^{-5}\,°C^{-1}$ to $2.0 \times 10^{-5}\,°C^{-1}$. The lowest value was chosen to examine the effects of soil thermal expansion on the thermal-mechanical behavior of the wall. As well as the friction angle, it was chosen at 30° as a conservative value for it falls in the range found in the literature reviews (30–36°) [36,38]. According to literature review [36], the dilation angle of dense sand and loose sand are from 0–12° and 0–10°, respectively. It was chosen at 4° as an intermediate value in the present study.

In order to simulate the heating phase performed in the experiment, the temperature of the pipes (the vertical line located inside the wall, see Fig. 2) was imposed. The initial temperature of the whole system was first fixed at 10 °C (following the experimental observation). To start the heating phase, the temperature of the pipe was increased from 10 °C to 48.5 °C following function (1):

$$T = \frac{2.07 \cdot t + 1.1615}{0.0414 \cdot t + 0.12323} \quad (1)$$

where t is elapsed time and T is temperature. This choice allows fitting the experimental data of the temperature measured by the sensor that is closest to the pipes (0.03 m from the pipe axis, on the left-hand side).

4. Result

In this section, the results obtained from physical test and numerical analysis are compared in the same figures.

Fig. 3 shows the temperature measured within the wall on the left-hand side in the plane of the wall panel at three different depths (0.33 m, 1.00 m and 1.67 m) and on the right-hand side at mid-plane (x = 1.00 m Fig. 1), versus elapsed time (the origin corresponds to the start of the heating phase). The symbols represent the experimental data (EXP) and the continuous lines represent the numerical results (NUM). Note that in the experiments, more than one sensor exists for one distance (see Fig. 1b). As an example, at y = 0.92 m on the left-hand side (Fig. 3) within the wall, there are three sensors on each depth (0.33 m and 1.67 m). The results obtained by these three sensors (showing an increase of temperature from 10 °C to 45 °C) have a difference of about 3–4 °C at the end of the heating phase. This difference

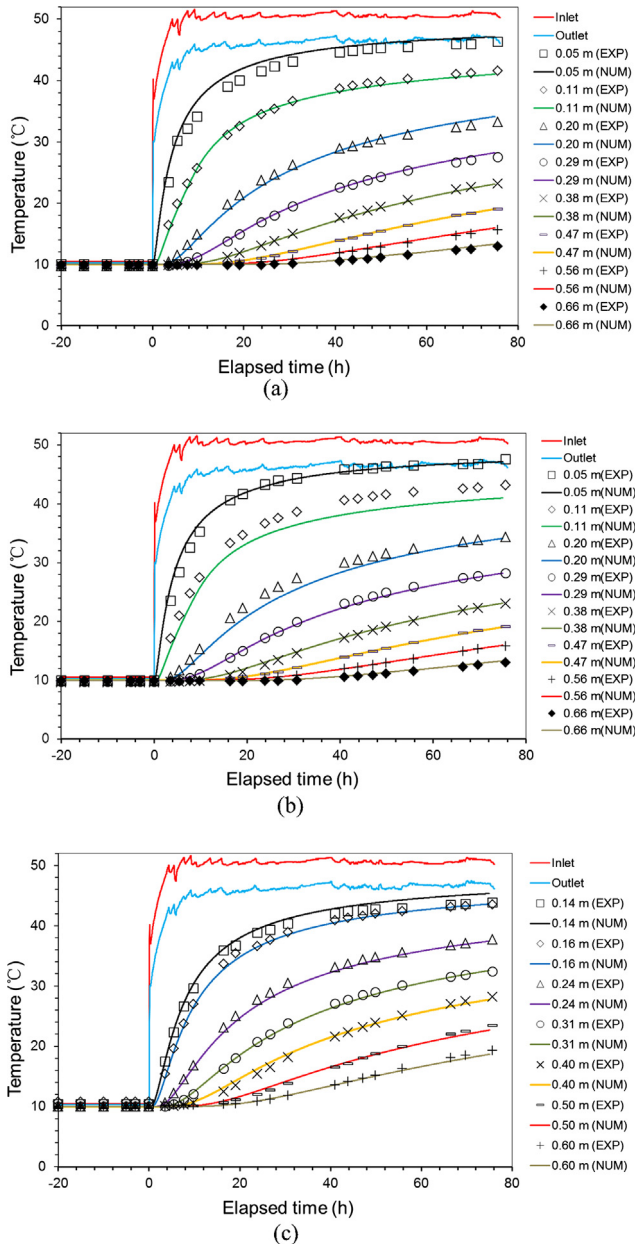

Fig. 4. Temperature versus elapsed time in the sand mass at various distances from the pipes axis: (a) on the left-hand side at x = 0.44 m; (b) on the left hand side at x = 1.56 m; (c) and on the right-hand side at x = 1.00 m.

can be explained by the gradual cooling of the fluid while circulating into the pipe which represents an ordinary characteristic condition of energy diaphragm wall.

Fig. 4 shows the temperature for each single line of sensors embedded in the sand. The agreement between the experimental data and the numerical results confirms that the numerical 2D finite element model is suitable to predict the heat transfer in sand in this experiment.

Fig. 5 shows the temperature profile measured at various moments. It can be seen that at a given time, the temperature at a location closer to the pipe is higher. This plot allows two zones to be distinguished: inside the wall, the temperature gradient is smaller than in the soil. That can be explained by the thermal conductivities of these materials and the boundary conditions: the wall, made of cement, is more conductive than the sand and therefore, the temperature gradient is then smaller.

The numerical results shown in Figs. 3–5 are in good agreement with the experimental results. That confirms, in this experiment, heat transfer is mainly governed by heat conduction (as considered in the numerical simulation). This agreement confirms also that the thermal boundary conditions used in the simulation are acceptable. In addition, as a 2D mesh was used in the simulation, the numerical results should be compared with the mean values obtained in the experiments with various sensors located at the same distance. The non-uniform of the temperature distribution along the X direction (observed from the experiments) can be ignored in the numerical model.

Fig. 6 shows the vertical strain (Z direction, see Fig. 1a) measured at various x coordinates by the strainmeters. Note that all the strainmeters on the left-hand side (Fig. 6a–c) are located 0.03 m from the pipe. The results show similar trends for all sensors; a rapid increase of strain during the first 20 h (corresponding to the increase of fluid temperature during the experiment) followed by a more stable phase. The final strain is in the range of 50–70 με (except one sensor at 0.33-m depth). The three sensors located at 0.33-m depth show larger strain variation than those at 1.67-m depth; there is only one sensor located at 1.00-m depth. On the right-hand side (Fig. 6d), only one sensor was used for each depth. Note that these sensors are located 0.06 m to the right-hand side of the pipes. The results obtained by these sensors are quite similar showing a quick increase during the first 20 h and stabilization at 55–65 με. These discrepancies in strains can be directly linked to the heterogeneity of temperature distribution of the wall shown in Fig. 6.

The vertical strains predicted by the numerical analysis are also shown in the Fig. 6 (positive strain corresponds to expansion). On the left-hand side, the numerical analysis show that heating induced a quick expansion at 0.33-m depth followed by stabilization at 80 με. This result is similar to that obtained by the experiment. However, for the other depth (1.67 m), the numerical analysis shows a contraction during the first hours. This contraction was then followed by expansion and the final values are also similar to the experimental ones. The trend of the vertical strains on the right-hand side shows a good agreement between the numerical and the experimental results.

The following mechanisms can be mentioned to explain these results (see also the vertical stress variation plotted in the Fig. 6). The high value of vertical stress is related to the temperature gradient in the wall thickness (see Fig. 1). When the temperature of the wall increases, the vertical strain increases by the thermal expansion. As the boundary condition at base of the domain was vertically fixed, the deformation of the wall could only expand upward. On the left-hand side, the heating rate is higher (so during the first 20 h), thermal expansion on the left-hand side is higher than the right-hand side. This thermal expansion in the left-hand side was then “restrained” by the right-hand side of the wall. At the same time, the vertical expansion of the wall mobilizes the shaft friction along its interface in contact with the soil mass. That mobilized shaft friction tends to prevent the wall vertical expansion, increasing then the vertical stress inside the wall. On the other hand, the sensors located at larger depths (1.67 m) are subjected to higher increase of vertical stress. That explains the compression of the wall during the first hours on the left-hand side at large depths and tensile stress on the right-hand side.

Fig. 7 shows the normal stress on soil-wall interface versus elapsed time at various locations. The initial value of the lateral earth pressure is approximately 1 kPa at 0.33 m depth, 5 kPa at 1.00 m depth and 9 kPa at 1.67 m depth. On the left-hand side (Fig. 7a), at 0.33-m depth, there is only one transducer. The measurement shows a quick increase of the earth pressure following the heating phase, and the value at stabilization is approximately 4 kPa. At 1.00-m depth, there are two sensors both showing a quick increase of the earth pressure and the final values are approximately 11 kPa. The discrepancies between the two sensors are around 1 kPa. The sensors at 1.67-m depth show similar trend with the final values close to 16 kPa. As a conclusion, for the left-hand side, the variation of earth pressure is more significant at greater depth during heating.

The general trend observed on the right-hand side is different at the

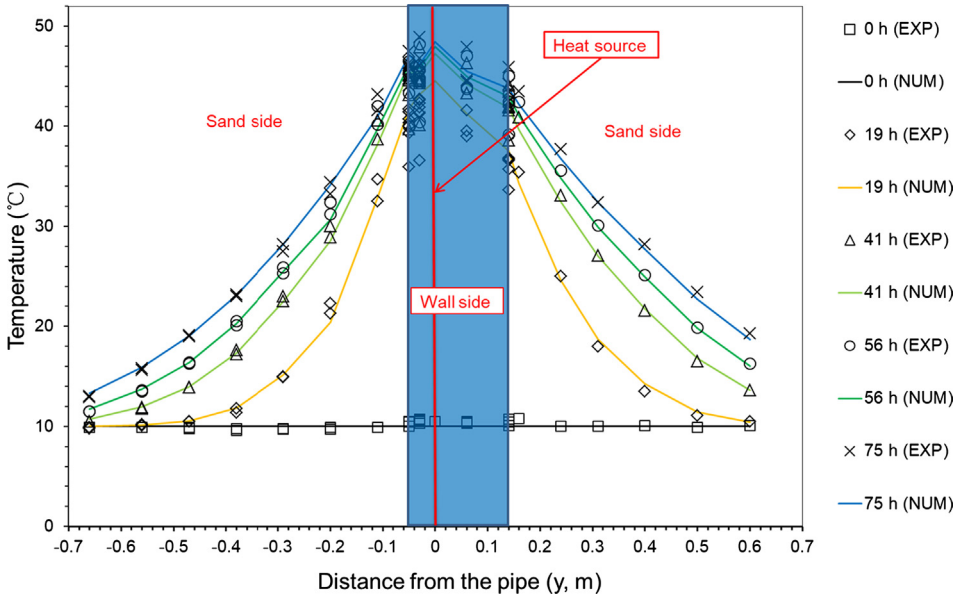

Fig. 5. Temperature versus distance from the pipe at various elapsed times in the middle of the panel (z = 1.00 m).

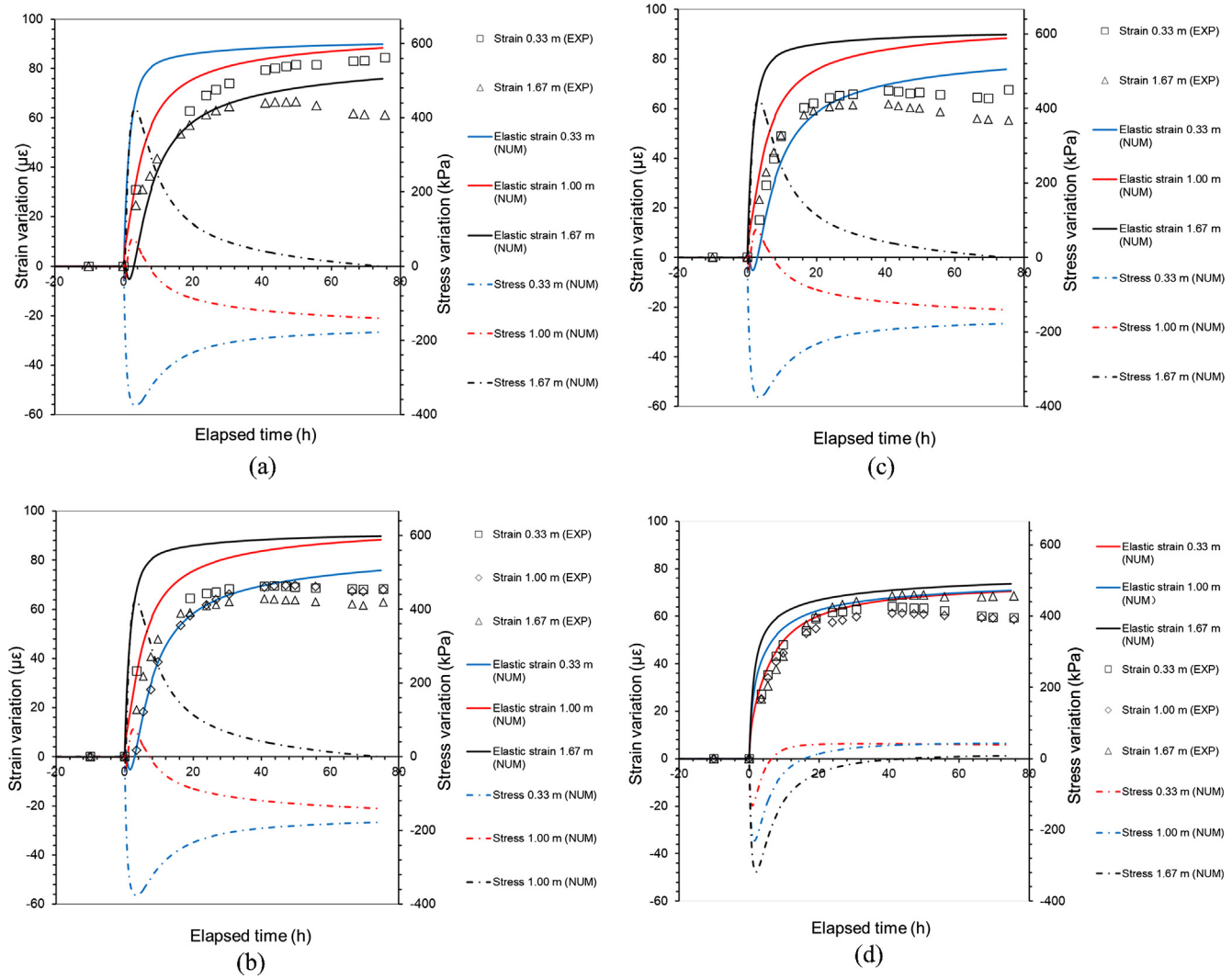

Fig. 6. Vertical strain and stress versus elapsed time on the left-hand side at (a) x = 0.28 m; (b) x = 1.00 m; (c) x = 1.72 m; (d) and on the right hand at x = 1.00 m.

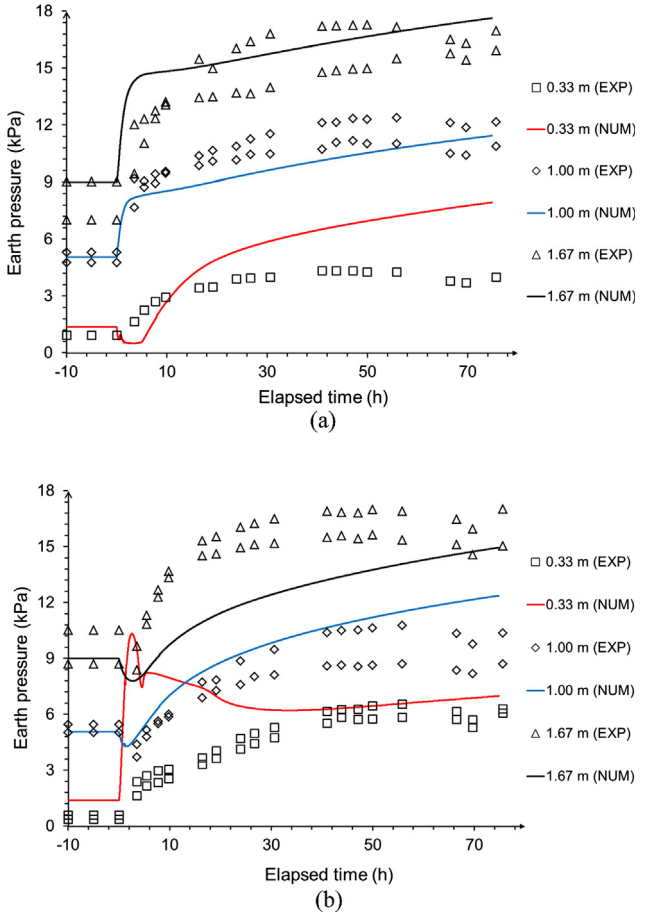

Fig. 7. Stress versus elapsed time at various depths on the left-hand side (a) and on the right-hand side (b).

start of heating (Fig. 7b). At 0.33-m depth, the two earth pressure sensors show quick increase with the heating and the final average value equals 6 kPa, with a discrepancy of less than 0.5 kPa. At 1.00-m depth, both sensors show first a decrease of the earth pressure during the first hours of heating. These values increase and reach around 9 kPa at the end (with a discrepancy of 1 kPa). For the sensors at 1.67-m depth, the earth pressure increases with the heating and reaches 15–17 kPa at the end. It could be seen there are still increase of pressure on both side at end of the test, this may due to a small temperature fluctuation of the heat sources.

The numerical results corresponding to the sensors at 1.00-m and 1.67-m depths show good agreement with the experimental ones for both sides. Even the decrease of the earth pressure at 1.00-m depth on the right-hand side was well predicted. However, the numerical results corresponding to lower depth (0.33 m) are different from the experiment values, especially during the few hours after heating. On the left-hand side, the numerical simulation shows a decrease of earth pressure during the first hour, which was not observed in the experiment. On the right-hand side, the earth pressure spikes during the first hour, which was not observed in the experiment. These problems would be explained by the stress-strain behavior of the sand at high strain rates under low stress level that could not be well predicted by FEA [39,40] and maybe also for the reason the sand was not so well compacted near the sand-concrete interface.

In order to better understand the results on the change of earth pressure (shown in Fig. 7), the deformed mesh (5 h after the starting of the heating) is shown in Fig. 8. Heating induces thermal expansion of the wall. That tends to increase the earth pressure at the soil/wall interface. However, as the pipes were located closer to the left-hand side, the temperature distribution is non-uniform. With the temperature on the left-hand side increasing more quickly than that on the right-hand side. This induces a bending of the wall that can be seen clearly in the Fig. 8. This bending contributes also to the modification of the earth pressure. Besides the increase of earth pressure related to the wall expansion, the wall bending decreases the earth pressure (mostly on the top) on the left-hand side and increases that on the right-hand side. That explains why the increase of earth pressure at 0.33-m depth on the right-hand side is higher than those at higher depth and the order is opposite on the left-hand side. In addition, the bending of the wall also explains the decrease of earth pressure observed at 1.00-m depth on the right-hand side during the first few hours.

5. Discussion

In the present work, a 1-g physical model was used to study the

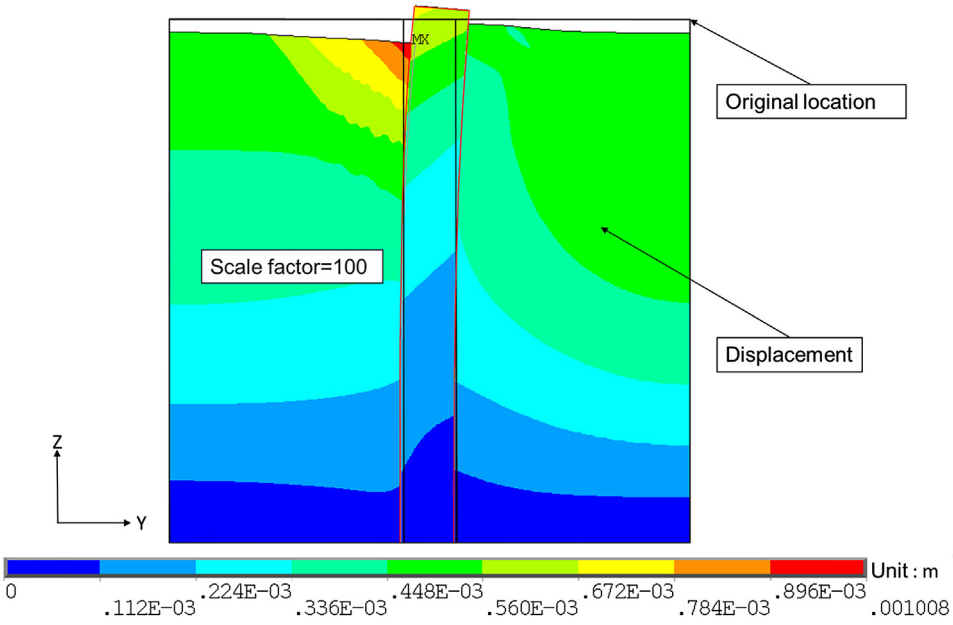

Fig. 8. Deformed mesh at 5 h (the color represents the sum of Y and Z displacement vectors).

thermo-mechanical behavior of an energy wall panel. Strainmeters were used to capture the axial strain inside the wall and earth pressure transducers were used to capture the normal stress at the soil/wall interface. This approach has been used in various studies to investigate the mechanical behavior of geostructures [41–43]. The results obtained in the present work show that this method could be also used to investigate the thermo-mechanical behavior of energy geostructures.

As far as the numerical model was concerned, the present study used a plane strain 2D FE model that approximates the conditions of the experiment. Even if this model could not capture the 3D heterogeneity of the temperature distribution, related to the difference between the inlet and outlet temperatures, a generally good agreement between the numerical and the experimental results can be observed. This confirms also that the boundary conditions and the constitutive laws used in this model are suitable for this case. Note that, for studying the thermal behavior of energy geostructures, usually only heat conduction is considered for heat transfer in the soil and in the reinforce concrete [29,30,44] unless ground water flow is present [7,45,46]. Heat convection in heat exchange pipe was discussed in the literature [32] and the heat transfer mechanism between the fluid and the pipe is more complex to be simulated [47,48]. The hypothesis of elastic deformation is usually used for gravel soils in numerical simulation because it is in agreement with experimental observations [27,29,49,50]. In some cases where clayey soils were considered, more complex constitutive laws maybe required [51–54]. As mentioned above, to simplify the model, the heat exchange pipe is often represented by a line with controlled temperature [26]; The thermo-mechanical behavior of the soil was assumed to be elastic and the effect of temperature on the soil mechanical properties was ignored.

Both numerical and experimental results obtained in the present work evidence that heating the diaphragm wall induces thermal expansion and this increases the lateral earth pressure applied on the wall surface. The lateral earth pressure could be three times larger than the initial stress value under low stress level. This variation seems to have a significant contribution to the vertical stress within the wall. Previous studies on energy pile indicate that radial contact pressures typically increase less than 5 kPa along 20 m depth of the pile under an increase of 25 °C of the pile temperature [33,34]. In real scale structures, the height to width ratio could be much higher than the ratio in this physical study (equal to 10). As a result, the increase of lateral earth pressures might be negligible with respect to the variations of vertical stresses. However, for an energy pile, the increase of this pressure is almost homogenous because the layout of the pipes is usually symmetric. For diaphragm walls, the behavior is more complex and strongly depends on the distribution of the heat exchange pipes inside the wall. The eccentric position of the heat exchanger loop caused a temperature gradient across the wall thickness, which leads to wall bending. This phenomenon exists also in the wall that is not fully embedded [31], since the temperature condition on the soil side is different from the temperature condition on the excavation side. This represents an additional contribution to thermally-induced vertical strains that are not uniform on the two sides of the wall.

6. Conclusions

The thermo-mechanical behavior of energy wall panel during heating was investigated using both physical and numerical models. The following conclusions can be drawn:

- Heating induces thermal expansion of the wall. The vertical thermal expansion mobilizes the shaft friction between the soil and the wall and then modifies the axial stress state inside the wall. Horizontal expansion increases the earth pressure at the soil/wall interface, and thus increases the mobilized shaft friction along the wall and the vertical stress inside the wall.
- As the pipe layout was not symmetric, thermal expansion bends the wall resulting in different stress/strain response between the two sides.
- A short-term heating of the wall shows a significant temperature gradient across the wall thickness. As a result, significant stress/strain variation is generated within the wall during the first few hours.
- The numerical model using an elastic law for the thermo-mechanical behavior of soil is appropriate to predict the behavior of the wall under thermal loading. There is however some discrepancy between experiment and numerical results that requires a deeper investigation, i.e. soil behavior at high strain rate under low stress level, 3D effect in the numerical model, etc.
- In spite of the temperature difference between the outlet and inlet fluid temperature, that induced a non-uniform temperature distribution inside the wall, a 2D numerical model seems appropriate to predict the main features of the panel's thermo-mechanical behavior observed by physical model.

Acknowledgement

This research was supported by the National Natural Science Foundation of China (grant number 41272314); and Science and Technology Project of Suzhou (grant number SYG201451); and the European Commission via the Marie Curie IRSES project GREAT 'Geotechnical and geological Responses to climate change: Exchanging Approaches and Technologies on a world-wide scale' (grant number FP7-PEOPLE-2013-IRSES-612665). Thanks are also due to Yinkang Zhou from Nanjing University for valuable discussion.

References

[1] H. Brandl, Energy foundations and other thermo-active ground structures, Géotechnique 56 (2) (2006) 81–122, https://doi.org/10.1680/geot.2006.56.2.81.
[2] L. Laloui, M. Nuth, Investigations on the mechanical behavior of a Heat Exchanger Pile, in: International Symposium on Deep Foundations on Bored and Auger Piles, London, 2009, pp. 343–347. http://doi.org/10.1201/9780203882870.ch39.
[3] Y.U. Chuang, L.Y. Pan, S.Y. Liu, Y.Q. Cai, Working mechanism and application of heat exchanger piles, Yantu Lixue/rock Soil Mech. 30 (4) (2009) 932–937 (In Chinese).
[4] H. Péron, C. Knellwolf, L. Laloui, A method for the geotechnical design of heat exchanger piles, ASTM, Geotechnical Special Publications (GSP), 2011, pp. 470–479.
[5] O. Boënnec, Piling on the Energy, Geodrilling Int. 150 (2009) 25–28.
[6] F. Dupray, C. Li, L. Laloui, Heat-exchanger piles for the de-icing of bridges, Acta Geotech. 9 (2014) 413–423, https://doi.org/10.1007/s11440-014-0307-2.
[7] M.E. Suryatriyastuti, H. Mroueh, S. Burlon, Impact of transient heat diffusion of a thermoactive pile on the surrounding soil, in: L. Laloui, A.D. Donna (Eds.), Energy Geostructures: Innovation in Underground Engineering. ISTELtd. and, John Wiley & Sons Inc, 2013, pp. 193–209.
[8] S. Kürten, D. Mottaghy, M. Ziegler, A new model for the description of the heat transfer for plane thermo-active geotechnical systems based on thermal resistances, Acta Geotech. 10 (2015) 219–229, https://doi.org/10.1007/s11440-014-0311-6.
[9] L. Laloui, M. Nuth, L. Vulliet, Experimental and numerical investigations of the behaviour of a heat exchanger pile, Int. J. Numer. Anal. Met. 30 (8) (2006) 763–781, https://doi.org/10.1016/S1571-9960(05)80040-0.
[10] P.J. Bourne-Webb, B. Amatya, K. Soga, T. Amis, C. Davidson, P. Payne, Energy pile test at Lambeth College, London: geotechnical and thermodynamic aspects of pile response to heat cycles, Géotechnique 59 (3) (2009) 237–248, https://doi.org/10.1680/geot.2009.59.3.237.
[11] J.S. McCartney, K.D. Murphy, Strain distributions in full-scale energy foundations (DFI young professor paper competition 2012), DFI J. Deep Found. Inst. 6 (2) (2012) 26–38, https://doi.org/10.1179/dfi.2012.008.
[12] K.D. Murphy, J.S. McCartney, K.S. Henry, Evaluation of thermo-mechanical and thermal behavior of full-scale energy foundations, Acta Geotech. 10 (2) (2015) 179–195, https://doi.org/10.1007/s11440-013-0298-4.
[13] L. Laloui, C. Cekerevac, Non-isothermal plasticity model for cyclic behaviour of soils, Int. J. Numer. Anal. Met. 32 (5) (2008) 437–460, https://doi.org/10.1002/nag.629.
[14] J.S. McCartney, J.E. Roseberg, A. Sultanova, Engineering performance of thermo-active foundation systems, in: C.M. Goss, J.B. Kerrigan, J. Malamo, M.O. McCarron, R.L. Wiltshire, (Eds.), GeoTrends: the Progress of Geological and Geotechnical Engineering in Colorado at the Cusp of a New Decade (GPP 6), 2010, pp. 27–42.
[15] J.S. McCartney, J.E. Rosenberg, Impact of heat exchange on the axial capacity of thermo-active foundations, in: J. Han, D.E. Alzamora (Eds.), Proceedings of geo-frontiers 2011 (GSP 211), ASCE, Reston, VA, 2011, pp. 488–498.
[16] A. Kalantidou, A.M. Tang, J.M. Pereira, G. Hassen, Preliminary study on the

mechanical behaviour of heat exchanger pile in physical model, Géotechnique 62 (11) (2012) 1047–1051, https://doi.org/10.1680/geot.11.T.013.
[17] M.A. Stewart, J.S. McCartney, Centrifuge modeling of soil-structure interaction in energy foundations, J. Geotech. Geoenviron. 140 (4) (2014) 04013044, https://doi.org/10.1061/(ASCE)GT.1943-5606.0001061.
[18] N. Yavari, A.M. Tang, J.M. Pereira, G. Hassen, Experimental study on the mechanical behaviour of a heat exchanger pile using physical modeling, Acta Geotech. 9 (3) (2014) 385–398, https://doi.org/10.1007/s11440-014-0310-7.
[19] C.A. Kramer, O. Ghasemi-Fare, P. Basu, Laboratory thermal performance tests on a model heat exchanger pile in sand, Geotech. Geol. Eng. 33 (2) (2015) 253–271, https://doi.org/10.1007/s10706-014-9786-z.
[20] J.C.I. Goode, J.S. McCartney, Centrifuge modeling of end-restraint effects in energy foundations, J. Geotech. Geoenviron. 141 (8) (2015) 04015034, https://doi.org/10.1061/(ASCE)GT.1943-5606.0001333.
[21] N. Yavari, A.M. Tang, J.M. Pereira, G. Hassen, Mechanical behaviour of a small-scale energy pile in saturated clay, Géotechnique 66 (11) (2016) 878–887, https://doi.org/10.1680/geot./15-T-026.
[22] N. Yavari, A.M. Tang, J.M. Pereira, G. Hassen, Effect of temperature on the shear strength of soils and soil/structure interface, Can. Geotech. J. 53 (7) (2016) 1186–1194, https://doi.org/10.1139/cgj-2015-0355.
[23] V.T. Nguyen, A.M. Tang, J.M. Pereira, Long-term thermo-mechanical behavior of energy pile in dry sand, Acta Geotech. 3 (2017) 1–9, https://doi.org/10.1007/s11440-017-0539-z.
[24] L. Laloui, M. Nuth, Numerical modelling of the behaviour of a heat exchanger pile, Revue européenne de génie civil 9 (5–6) (2005) 827–839, https://doi.org/10.1080/17747120.2005.9692787.
[25] A.F. Rotta Loria, A. Gunawan, C. Shi, L. Laloui, C.W.W. Ng, Numerical modelling of energy piles in saturated sand subjected to thermo-mechanical loads, Geomech. Eng. Environ. 1 (2015) 1–15, https://doi.org/10.1016/j.gete.2015.03.002.
[26] N. Yavari, A.M. Tang, J.M. Pereira, N. Yavari, A simple method for numerical modelling of energy pile's mechanical behavior, Géotechnique Lett. 4 (April-June) (2014) 119–124, https://doi.org/10.1680/geolett.13.00053.
[27] M.E. Suryatriyastuti, H. Mroueh, S. Burlon, Understanding the temperature-induced mechanical behaviour of energy pile foundations, Renew. Sust. Energy Rev. 16 (5) (2012) 3344–3354, https://doi.org/10.1016/j.rser.2012.02.062.
[28] D. Salciarini, F. Ronchi, E. Cattoni, C. Tamagnini, Thermomechanical effects induced by energy piles operation in a small piled raft, Int. J. Geomech. 15 (2) (2013) 04014042, https://doi.org/10.1061/(ASCE)GM.1943-5622.0000375.
[29] E.H.N. Gashti, M. Malaska, K. Kujala, Evaluation of thermo-mechanical behaviour of composite energy piles during heating/cooling operations, Eng. Struct. 75 (2014) 363–373, https://doi.org/10.1016/j.engstruct.2014.06.018.
[30] B.L. Amatya, K. Soga, P.J. Bourne-Webb, Thermo-mechanical behaviour of energy piles, Géotechnique 62 (6) (2012) 503–519, https://doi.org/10.1680/geot.10.P.116.
[31] P.J. Bourne-Webb, T.M.B. Freitas, R.A.D.C. Gonçalves, Thermal and mechanical aspects of the response of embedded retaining walls used as shallow geothermal heat exchangers, Energy Build. 125 (2016) 130–141, https://doi.org/10.1016/j.enbuild.2016.04.075.
[32] D. Sterpi, A. Coletto, L. Mauri, Investigation on the behaviour of a thermo-active diaphragm wall by thermo-mechanical analyses, Geomech. Eng. Environ. 9 (2017) 1–20, https://doi.org/10.1016/j.gete.2016.10.001.
[33] C.G. Olgun, T.Y. Ozudogru, C.F. Arson, Thermo-mechanical radial expansion of heat exchanger piles and possible effects on contact pressures at pile–soil interface, Géotechnique Lett. 4 (3) (2014) 170–178, https://doi.org/10.1680/geolett.14.00018.
[34] T.Y. Ozudogru, C.G. Olgun, C.F. Arson, Analysis of friction induced thermo-mechanical stresses on a heat exchanger pile in isothermal soil, Geotech. Geol. Eng. 33 (2) (2015) 357–371, https://doi.org/10.1007/s10706-014-9821-0.
[35] S. Yin, B.F. Towler, M.B. Dusseault, L. Rothenburg, Numerical experiments on oil sands shear dilation and permeability enhancement in a multiphase thermoporoelastoplasticity framework, J. Petrol. Sci. Eng. 69 (3) (2009) 219–226, https://doi.org/10.1016/j.petrol.2009.08.017.
[36] S. Karthigeyan, V. Ramakrishna, K. Rajagopal, Influence of vertical load on the lateral response of piles in sand, Comput. Geotech. 33 (2) (2006) 121–131, https://doi.org/10.1016/j.compgeo.2005.12.002.
[37] M.L. Allan, Materials characterization of superplasticized cement–sand grout, Cem. Concr. Res. 30 (6) (2000) 937–942, https://doi.org/10.1016/S0008-8846(00)00275-1.
[38] L. Hazzar, M. Nhussien, M. Karray, Influence of vertical loads on lateral response of pile foundations in sands and clays, J. Rock. Mech. Geotech. Eng. 9 (2) (2017) 291–304, https://doi.org/10.1016/j.jrmge.2016.09.002.
[39] M. Omidvar, M. Iskander, S. Bless, Stress-strain behavior of sand at high strain rates, Int. J. Impact Eng. 49 (2) (2012) 192–213, https://doi.org/10.1016/j.ijimpeng.2012.03.004.
[40] F.L. Peng, F.L. Li, Y. Tan, FEM simulation of deformation and strength characteristics in geogrid-reinforced sand retaining wall under the change of loading rate, Proceedings of Geo-Frontiers 2011 International Conference (2011) 3807–3817.
[41] S.B. Reddy, A.M. Krishna, Recycled tire chips mixed with sand as lightweight backfill material in retaining wall applications: an experimental investigation, Int. J. Geosynth. Ground Eng. 1 (4) (2015) 31, https://doi.org/10.1007/s40891-015-0036-0.
[42] K.H. Lee, J.Y. Cho, R. Salgado, I. Lee, Retaining wall model test with waste foundry sand mixture backfill, Geotech. Test J. 24 (2001) 401–408, https://doi.org/10.1520/GTJ11137J.
[43] H. Schad, P.A. Vermeer, A. Lächler, Fresh concrete pressure in diaphragm wall panels and resulting deformations, in: Ch.U. Grosse (Ed.), Advances in Construction Materials, Springer Verlag, Berlin, 2007, pp. 505–512.
[44] M. Sun, C. Xia, G. Zhang, Heat transfer model and design method for geothermal heat exchange tubes in diaphragm walls, Energy Build. 61 (6) (2013) 250–259, https://doi.org/10.1016/j.enbuild.2013.02.017.
[45] A.D. Donna, M. Barla, The role of ground conditions on energy tunnels' heat exchange, ICE Env. Geotech. 3 (2016) 214–224, https://doi.org/10.1680/jenge.15.00030.
[46] F. Dupray, M. Bachler, L. Laloui, Effect of groundwater flow on the THM behavior of an energy pile, in: M. Manassero, A. Dominijanni, S. Foti, G. Musso (Eds.), Coupled Phenomena in Environmental Geotechnics, CRC Press, 2013, pp. 483–489, , https://doi.org/10.1201/b15004-63.
[47] B. Dubroca, G. Duffa, B.Leroy, High temperature mass and heat transfer fluid-solid coupling, in: 11th Meeting AIAA/AAAF Space Planes and Hypersonic Systems and Technologies, Orleans, France, 2002, p. 5124.
[48] R.R.E. Khoury, M. Errera, K.E. Khoury, M. Nemer, Efficiency of coupling schemes for the treatment of steady state fluid-structure thermal interactions, Int. J. Therm. Sci. 115 (2017) 225–235, https://doi.org/10.1016/j.ijthermalsci.2017.02.001.
[49] S. Jeong, H. Lim, J.K. Lee, J. Kim, Thermally induced mechanical response of energy piles in axially loaded pile groups, Appl. Therm. Eng. 71 (1) (2014) 608–615, https://doi.org/10.1016/j.applthermaleng.2014.07.007.
[50] L. Laloui, Thermo-mechanical behaviour of soils, Revue Française De Génie Civil 5 (6) (2001) 809–843.
[51] C. Cekerevac, L. Laloui, Experimental study of thermal effects on the mechanical behaviour of a clay, Int. J. Numer. Anal. Met. 28 (3) (2004) 209–228, https://doi.org/10.1002/nag.332.
[52] L. Laloui, C. Cekerevac, B. François, Constitutive modelling of the thermo-plastic behaviour of soils, Revue Européenne De Génie Civil 9 (5–6) (2005) 635–650.
[53] A.M. Tang, Y.J. Cui, N. Barnel, Thermo-mechanical behaviour of a compacted swelling clay, Géotechnique 58 (1) (2008) 45–54, https://doi.org/10.1680/geot.2008.58.1.45.
[54] P.Y. Hong, J.M. Pereira, A.M. Tang, Y.J. Cui, On some advanced thermo-mechanical models for saturated clays, Int. J. Numer. Anal. Met. 37 (2013) 2952–2971, https://doi.org/10.1002/nag.2170.